Bioavailability and molecular recognition between secondary metabolites of *Euphorbia hirta* L. and 5-lipoxygenase using fragment molecular orbital method and pair interaction energy decomposition analysis

Biodisponibilidad y reconocimiento molecular entre metabolitos secundarios de *Euphorbia hirta* L. y 5-lipoxigenasa usando el método de orbitales moleculares de fragmentos y análisis de descomposición energética de interacción de pares

Emildo Marcano[*,1], Ysbelia Sánchez[**,2]

Abstract

Is presented the bioavailability analysis for seven secondary metabolites from *Euphorbia hirta* L. (Euphorbiaceae). The bioactivity score, the molecular similarity analysis for each secondary metabolite, and the molecular docking 5-LOX/metabolite complex are also presented. For the similarity analysis, it is referenced the structure of allosteric LOX-5 inhibitor 3-acetyl-11-keto-beta-boswellic acid (AKBA). The fragment molecular orbital method (FMO) and pair interaction energy decomposition analysis (PIEDA) were applied to evaluate the interaction energy between secondary metabolites and the 5-LOX active site. Log P values of all the secondary metabolites studied were found to be higher than 5, contrary to what was expected with Lipinski's rules of five. The reference LOX-5 ligand has a high electrostatic potential similarity with most secondary metabolites studied, with values from 0.667 to 0.730. Both, AKBA and metabolites ligands were wedged between the two domains of LOX-5, and the main residues contact were LEU-66, ARG-68, VAL-110, HIS-130, ILE-126, GLN, 129 and LYS-133. The PIEDA analysis showed that stabilization in the 5-LOX active site is mainly dominated by hydrophobic interactions, with values up to -35 Kcal/mol. Due to the low presence of terminal-OH groups, electrostatic origin and charge transfer interaction energies are also important but have values of less than 20 Kcal/mol.

Keywords: *Euphorbia hirta* L., LOX-5 inhibitor, PIEDA analysis, FMO, bioactivity score, molecular similarity analysis, molecular docking

Resumen

Se reporta el análisis de biodisponibilidad de siete metabolitos secundarios de *Euphorbia hirta* L. (Euphorbiaceae). Además, se presenta la puntuación de bioactividad, el análisis de similitud molecular para cada metabolito secundario y el acoplamiento molecular del complejo 5-LOX/metabolito. Para el análisis de similitud, se utilizó como referencia la estructura del inhibidor alostérico de LOX-5, el ácido 3-acetil-11-ceto-beta-boswélico (AKBA). Se aplicó el método de orbitales moleculares de fragmentos (FMO) y el análisis de descomposición de energía de interacción de pares (PIEDA) para evaluar la energía de interacción entre los metabolitos secundarios y el sitio activo 5-LOX. Se encontró que los valores de Log P de todos los metabolitos secundarios estudiados eran superiores a 5, contrariamente a lo esperado con las reglas de cinco de Lipinski. El ligando LOX-5 de referencia tiene una alta similitud de potencial electrostático con la mayoría de los metabolitos secundarios estudiados, con valores de 0,667 a 0,730. Tanto los ligandos de AKBA como los de sus metabolitos estaban encajados entre los dos dominios de LOX-5, y los principales residuos en contacto fueron LEU-66, ARG-68, VAL-110, HIS-130, ILE-126, GLN, 129 y LYS-133. El análisis PIEDA mostró que la estabilización en el sitio activo de 5-LOX está dominado principalmente por interacciones hidrofóbicas, con valores de hasta -35 Kcal/mol. Las energías de interacción de origen electrostático y de transferencia de carga también son importantes, pero tienen valores inferiores a 20 Kcal/mol, debido a la baja presencia de grupos -OH terminales.

Palabras clave: *Euphorbia hirta* L., Inhibidor de LOX-5, análisis PIEDA, FMO, índice de bioactividad, análisis de similitud molecular, acoplamiento molecular

* Departamento de Química. Laboratorio de Computación de Alto Rendimiento **Laboratorio de Investigaciones Genéticas. Universidad Nacional Experimental del Táchira (UNET), Venezuela. Correspondencia: jedi148@gmail.com

Orcid: [1]0000-0002-7235-8533
[2]0000-0002-0142-1208

Introduction

Leukotrienes (LT) are lipid mediators that are pivotal in acute and chronic inflammation and allergic diseases linked to asthma and atherosclerosis. LT biosynthesis is initiated by 5-lipoxygenase (5-LOX) with the assistance of the substrate-binding 5-LOX-activating protein at the nuclear membrane (Rådmark and Samuelsson, 2009). LOX enzymes from mammals consist of two domains. An N-terminal regulatory C2-like domain (residues 1–112 in 5-LOX) mainly consists of β-sheets, and a C-terminal catalytic domain (residues 126–673 in 5-LOX) is mainly helical in structure and contains iron (Rådmark et al., 2015). The products of 5-lipoxygenase are synthesized and released in the airway when an asthmatic reaction occurs. 5-lipoxygenase, via arachidonic acid metabolism, produces leukotrienes that mediate bronchoconstriction and inflammatory modifications essential in the pathophysiology of asthma. In the past, arachidonate 5-lipoxygenase inhibitors have been investigated to attenuate the activity of 5-LOX. Many of these inhibitors are based on natural product extracts. For example, pharmacological testing revealed human 5-lipoxygenase as a molecular target of the predatory myxobacterium Pyxidicoccus fallax HKI 727 myxochelins extracts. In particular, myxochelin A efficiently inhibited 5-LOX activity with an IC50 of 1.9 μM (Schieferdecker et al., 2015). In the case of plants, extracts from many species have also been investigated for inflammatory response and 5-LOX inhibition (Lončarić et al., 2021; Gadnayak et al., 2022; Liu et al., 2023), highlighting pentacyclic triterpenes as a rich natural resource of promising compounds for drug development. Therefore, the inhibitory activities of 29 natural oleanane and ursane pentacyclic triterpenes were evaluated against the 5-LOX activity, and the analysis of the structure-activity relationships revealed that the presence of a hydroxy was beneficial in terms of the inhibition (Quynh Vo et al., 2019). Lipoxygenase inhibition and molecular docking studies of secondary metabolites from the leaves of *Alstonia scholaris* has been reported. Molecular docking results identified the main interaction sites HIS 518 and GLN 514 (Ghansenyuy et al., 2023).

Specifically, and for our interest, ethanol *Euphorbia hirta* L. (Euphorbiaceae) leaf extract exhibited significant anti-inflammatory activity than root by inhibiting albumin denaturation, proteinase, and the lipoxygenase activities with 87.51 %, and 51.2 % followed by 97.30 %, and 54.21 % followed by 94.43 % and 48.21 %, respectively, at 100 μg/mL (Das et al., 2022). *Euphorbia hirta* L. is one of the common plants in the subtropical region and is considered a weed distributed to the hotter parts of tropical and sub-tropical countries. *Euphorbia hirta* L. is an erect or decumbent herb 40 to 60 cm long, with simple, opposite leaves with red spots. The inflorescence on the fruit is capsule-shaped and has white latex. In the last years, the secondary metabolites from the genus Euphorbia have been highlighted as potential compounds for drug design with different molecular targets (Shi et al., 2008), and antimicrobial, anti-inflammatory, anti-amoebic, antifertility, anti-malarial, antioxidant, sedative, cytotoxic, aflatoxin inhibition, larvicidal, immunomodulatory, and other properties were reported (Verma, 2017).

Most studies on the anti-inflammatory properties of Euphorbia secondary metabolites are based on *in vivo* results.

Thus, to contribute to the molecular perspective of these compounds, we report the bioavailability analysis for seven secondary metabolites from *Euphorbia hirta* L. previously reported (Shi et al., 2008). The bioactivity score, the molecular similarity analysis for each secondary metabolite, and the molecular docking 5-LOX/metabolite complex are also presented. To solve the lack of computational resources for applying molecular dynamics simulations, we have applied the fragment molecular orbital method (FMO) and pair interaction energy decomposition analysis (PIEDA) to evaluate the interaction energy between secondary metabolites and the 5-LOX active site.

Computational details

2.1 Geometric Optimization and Molecular Similarity Analysis

The molecular similarity principle states that molecules with similar structures tend to have similar properties (Bender and Glen, 2004). Indeed, the observation that common sub-structural fragments lead to similar biological activities can be quantified from database analysis (Eckert and Bajorath, 2007). The secondary metabolites studied are shown in Figure 1. These compounds are triterpenes extracted from *Euphorbia hirta* L., whose cytotoxic and antimicrobial potentials have been documented (Ragasa and Cornelio, 2013).

For the similarity analysis, we used as a reference the structure of allosteric LOX-5 inhibitor 3-acetyl-11-keto-beta-boswellic acid (AKBA) (Gilbert et al., 2020). For all structures, the geometric optimizations were carried out at the DFT CAM-B3LYP/6-31(d) level using the GAMESS software

package (Schmidt et al., 1993) on the ChemCompute website (Perri and Weber, 2014). The molecular similarity calculations were carried out with the ShaEP software package. ShaEP performs rigid-body superimposition of 3D molecular models using a matching algorithm (Vainio et al., 2009). Two characteristic scores were calculated for comparison: 3D shape and electrostatic potential (ESP) (Shin et al., 2015). These scores range from 0 to 1, in which 0 and 1 correspond to no similarity and the same molecules. As a complement to the ShaEP results, the ESP mapped was obtained at the DFT CAM-B3LYP/6-31(d) level.

2.2 Bioavailability prediction

Properties of molecules such as bioavailability or membrane permeability have often been connected to simple molecular descriptors such as logP (partition coefficient), molecular weight (MW), or counts of hydrogen bond acceptors and donors in molecule (Muegge, 2003). These descriptors are included in the Lipinski "Rule of Five" (Lipinski et al., 1997). The rule states that most molecules with good membrane permeability have logP ≤ 5, molecular weight ≤ 500, hydrogen bond acceptors ≤ 10, and hydrogen bond donors ≤ 5. To evaluate the bioavailability of the secondary metabolites studied, the Lipinski´s parameters were calculated using Molinspiration Cheminformatics software (Molinspiration, 1986).

2.3 Preparation of LOX-5 protein and molecular docking

The allosteric inhibitor 3-acetyl-11-keto-beta-boswellic acid (AKBA) from
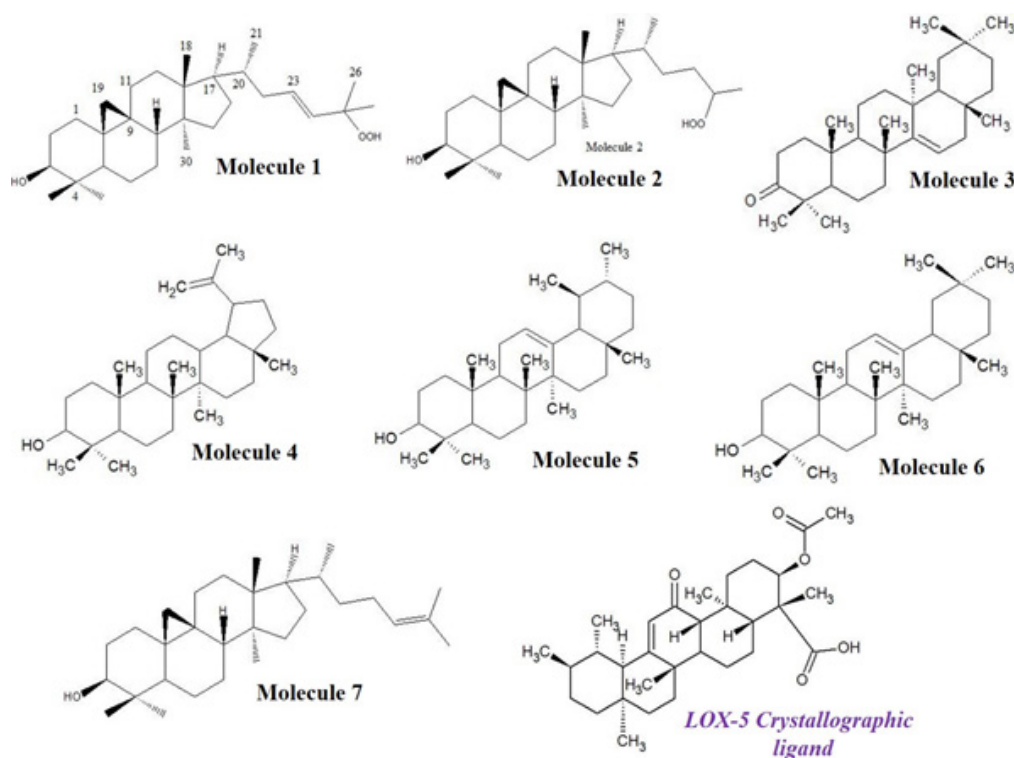
Figure 1. Triterpenes secondary metabolites studied and AKBA LOX-5 ligand reference

frankincense wedges between the membrane-binding and catalytic domains of LOX-5, some 30Å from the catalytic iron (PDB ID: 6NCF) (Gilbert et al., 2020). It was used to study the interaction with the triterpene's secondary metabolites from *Euphorbia hirta* L. We retained a LOX-5 AKBA complex consisting of 676 residues from the tetrameric PDB structure, from SER-15 to ILE-673. Hydrogen atoms were added to the model using the VEGA ZZ package (Pedretti et al., 2004). Atomic charges were assigned using the Gasteiger-Marsili method (Gasteiger and Marsili,1980). AKBA ligand, catalytic iron, water, and other crystal molecules were removed. Secondary metabolites from *Euphorbia hirta* L. were optimized using CAM-B3LYP/6-31(d) DFT level. Later, the ligands were prepared for docking experiments defining rotatable bonds using AutoDock Tools version 1.5.6. A grid box size of 40, 40, and 40 Å was generated and allocated at the center of

the receptor/binding site using x, y, and z coordinates of 0.285, 0.047, and -0.004, respectively. Molecular docking simulations of all structures were performed using AutoDockVina software (Trott and Olson, 2010) VEGAZZ was used to visualize all structures. A co-crystallized AKBA ligand was docked to validate the docking protocol. Finally, the major interaction mode (from energy affinity) was analyzed for each structure studied with the fragment molecular orbital method (FMO).

2.4. FRAGMENT MOLECULAR ORBITAL METHOD (FMO)

The FMO method is a general quantum chemical method and is one of the most efficient approaches for studying biomolecules. In the FMO method, a protein can be divided into smaller pieces called fragments or monomers; for example, each

residue can be represented as a fragment (Gonzalez and Mroginski, 2019). As a result of FMO calculations, we can obtain the interaction energy between interacting monomer pairs, which is advantageous because it allows the estimation of PIEs, describing the strength of the interaction between individual fragments (Fedorov and Kitaura, 2012). Then, Pair Interaction Energy Decomposition Analysis (PIEDA) can gain valuable insights into the chemical nature of noncovalent interactions between proteins and ligands. Noncovalent interactions such as salt bridges, hydrogen bonds, or polar interactions are dominated by the electrostatic and charge-transfer terms, while hydrophobic interactions are dominated by the dispersion term (Fedorov and Kitaura, 2006). For each triterpene studied (Figure 1), the major interaction mode for LOX-5/ligand complex was optimized at B3LYP/6-31(d) DFT level and then analyzed with the fragment molecular orbital method (FMO) at the same theory level, using GAMESS. The fragmentation, FMO input files and PIEDA values visualization analysis were carried out for all interaction modes using the Facio program interface tool (Suenaga, 2005). The Grimme's dispersion correction was added.

Results and Discussion

3.1 Bioavailability (Lipinski parameters)

Lipinski's rule is widely used to determine molecular properties important for a drug's pharmacokinetic *in vivo*. Table I contains the calculated molecular polar surface area (TPSA) and Lipinski's parameters of the *Euphorbia hirta* L. secondary metabolites investigated.

Molecular hydrophobicity or lipophilicity is indicated by the octanol/water partition coefficient (Log P). Drug molecules' hydrophilic/lipophilic nature affects drug permeability across the cell membranes. Log P values of all the secondary metabolites studied were found to be higher than 5, contrary to what was expected with Lipinski's rules of five. However, the log P values obtained are comparable to those reported for triterpenoids interacting with 11-Hydroxysteroid dehydrogenase type2 (Yamaguchi et al., 2011). According to theoretical and experimental reports, these compounds are described as lipophilic and high permeability structures (Wang et al., 2015; Bennion et al., 2017).

Total polar surface area (TPSA) is closely related to the hydrogen bonding potential of a molecule. It is a good predictor of drug transport properties such as intestinal absorption, bioavailability and blood-brain barrier penetration (Pajouhesh and Lenz, 2005). Molecules with a polar surface area greater than 140 $Å^2$ tend to be poor at permeating cell membranes (Nielsen et al., 2017). For molecules to penetrate the blood-brain barrier, a PSA of less than 90 $Å^2$ is usually needed (Hitchcock and Pennington, 2006). TPSA of molecules studied was found in the range of 20-81 $Å^2$, which agrees with the above mentioned limits (Table I). Therefore, all triterpenes of Figure 1 show a good capacity to penetrate the blood-brain barrier. Also, the TPSA values obtained agree with those reported for triterpenoids from *Vernonia patula* Merr. interacting with Cannabinoid Type 1 Receptor (Siraj et al., 2021). Several rotatable bonds are a simple topological parameter that measures molecular flexibility and is considered a

Table I.
Calculated molecular polar surface area (TPSA), and Lipinski parameters of the
Euphorbia hirta L. secondary metabolites investigated

Molecule	Volume	TPSA	Nrot	n ON accept	n OHNH donors	Log P	MW
LOX-5 cristal ligand	493.94	80.67	3	5	1	6.15	498.7
1	477.97	49.69	5	3	2	7.05	458.73
2	478.85	49.69	6	3	2	7.17	458.73
3	454.84	17.07	0	1	0	7.84	424.71
4	461.6	20.23	1	1	1	8.29	426.73
5	461.05	20.23	0	1	1	8.08	426.73
6	460.7	20.23	0	0	1	8.02	426.73
7	461.26	20.23	4	4	1	8.21	426.73

good descriptor of the oral bioavailability of drugs. It has been shown that higher oral bioavailability is associated with lower rotatable bond count. Rotational bonds make the compounds flexible; hence, they easily interact with specific rigid binding areas (Veber et al., 2002). The 1, 2, and 7 structures studied show lower molecular flexibility due to the range of rotatable bonds (4-6) than the crystallographic ligand for LOX-5. On the other hand, molecules 3, 5, and 6 do not show rotatable bonds. Therefore, these molecules are expected to show less molecular flexibility and less interaction with specific rigid binding areas in LOX-5. The number of hydrogen bond acceptors (O and N atoms) and the number of hydrogen donors (NH and OH) in the tested compounds were within Lipinski's limit, i.e., less than 10 and 5, respectively.

3.2 BIOACTIVITY SCORE

The predicted bioactivity scores of studied compounds (G protein-coupled receptors (GPCRs) ligand, ion channel modulator, kinase inhibitor, nuclear receptor ligand, protease inhibitor, and enzyme inhibitory activity), as well as their comparison with the crystallographic ligand for LOX-5 are summarized in Table II. As a general rule, the larger the bioactivity score, the higher the probability that the investigated compound will be active. Therefore, a molecule with a bioactivity score of more than 0.00 will likely possess considerable biological activities. At the same time, values from 0.50 to 0.00 are expected to be moderately active; if the score is less than -0.50, it is presumed inactive (Ochieng et al., 2017).

Table II shows that the triterpenes metabolites studied can act primarily as nuclear receptor ligands and other enzyme inhibitors. Additionally, these molecules also can act moderately as GPCR ligands. Nuclear receptors are transcription factors actively involved in many aspects of human physiology and pathology, serving as sensors of stimuli, master regulators of downstream molecular events, and hubs governing complex gene regulatory networks (Zhao et al., 2019). The identification of bioactive triterpenes as putative ligands in nuclear receptors has been reported in the past (Grienke et al.,

Table II.
Predicted bioactivity scores of the secondary metabolites investigated

Molecule	GPCR ligand	Ion channel modulator	Kinase inhibitor	Nuclear receptor ligand	Protease inhibitor	Enzyme inhibitor
LOX-5 cristal ligand	0.07	0.01	-0.68	0.67	0.16	0.56
1	0.34	0.09	-0.33	0.85	0.15	0.74
2	0.21	0.07	-0.4	0.84	0.1	0.74
3	0.07	-0.1	-0.4	0.43	-0.14	0.37
4	0.27	0.11	-0.42	0.85	0.15	0.52
5	0.22	-0.02	-0.41	0.79	0.19	0.6
6	0.22	-0.05	-0.31	0.67	0.11	0.56
7	0.21	0.1	-0.4	0.86	0.14	0.66

2011). In the case of the LOX-5 enzyme, the structure-activity relationships of pentacyclic triterpenoids as inhibitors have been reported, emphasizing the importance of the presence of hydroxyl and carboxylic acid groups in this interaction (Quynh Vo et al., 2019).

3.3 MOLECULAR SIMILARITY

The aim of this work is to explore the inhibitor potential of the secondary metabolites from *Euphorbia hirta* L. (Figure 1) against LOX-5, taking as reference the crystallographic ligand recently reported and available from the Protein Data Bank (Gilbert et al., 2020). Starting from the knowledge of this crystallographic ligand, we analyzed the molecular similarity between the triterpene metabolites of *Euphorbia hirta* L. Two important properties, 3D shape, and electrostatic potential (ESP) of secondary metabolites, were compared with the reference ligand, and the results are shown in Table III.

It is shown that the secondary metabolites studied have a good shape similarity with the reference ligand with values from 0.571 (molecule 1) to 0.695 (molecule 3). These molecules possess a similar framework of rings, substituted in some cases for –OH groups and unsaturated chains. The substitution of unsaturated chains in molecules 1, 2, and 7 is responsible for the decrease in the 3D shape values. It is also shown that the reference LOX-5 ligand has a high ESP similarity with most secondary metabolites studied, with values from 0.667 to 0.730. As a complement to the ESP results in Table III, Figure 2 shows the ESP mapped obtained at B3LYP/6-31(d) DFT level.

The high ESP similarity in these compounds and the reference ligand may be due to hydroperoxyl (-ROOH) and -OH functional groups close to the molecular ring framework. On these functional groups is spread the region of negative electrostatic potential, specifically on the lone pair oxygen atoms. Therefore, these oxygen atoms can be identified as reactive zones of

Table III.
3D-shape, electrostatic potential (ESP) and average for the secondary metabolites investigated

Molecule	Reference: LOX-5 crystallographic ligand		
	3D-Shape	*ESP*	*Average*
1	0.571	0.762	0.667
2	0.557	0.779	0.668
3	0.695	0.660	0.677
4	0.619	0.798	0.709
5	0.634	0.826	0.730
6	0.638	0.795	0.717
7	0.581	0.765	0.673

the molecules studied (Anzline et al., 2020). Thus, it is expected that when the molecules of Figure 1 come near the LOX-5 active site, these are attracted, and a charge transfer occurs between the different molecules involved. This process continues until the electrophilicity of the two molecules gets equal and after that there will be no interaction or transfer of charges (Anzline et al., 2017). Finally, when the 3D shape and ESP values are averaged, we observed a high similarity of the metabolites studied with the LOX-5 reference ligand.

3.4 MOLECULAR DOCKING

As an observer in Table III, the molecular similarity of triterpenes studied suggests these molecules could also interact with the LOX-5 active site. Therefore, in the present study, molecular docking was performed to identify the docking score of seven structures of Figure 1 towards the active site of the allosteric inhibitor 3-acetyl-11-keto-beta-boswellic acid (AKBA) recently reported (Gilbert et al., 2020). Figures 3a and 3b show the redocking results for the reference AKBA ligand previously optimized at CAM-B3LYP/6-31(d) DFT level.

As expected, the ligands were wedged between the two domains of LOX-5, and the main residues contact were LEU-66, ARG-
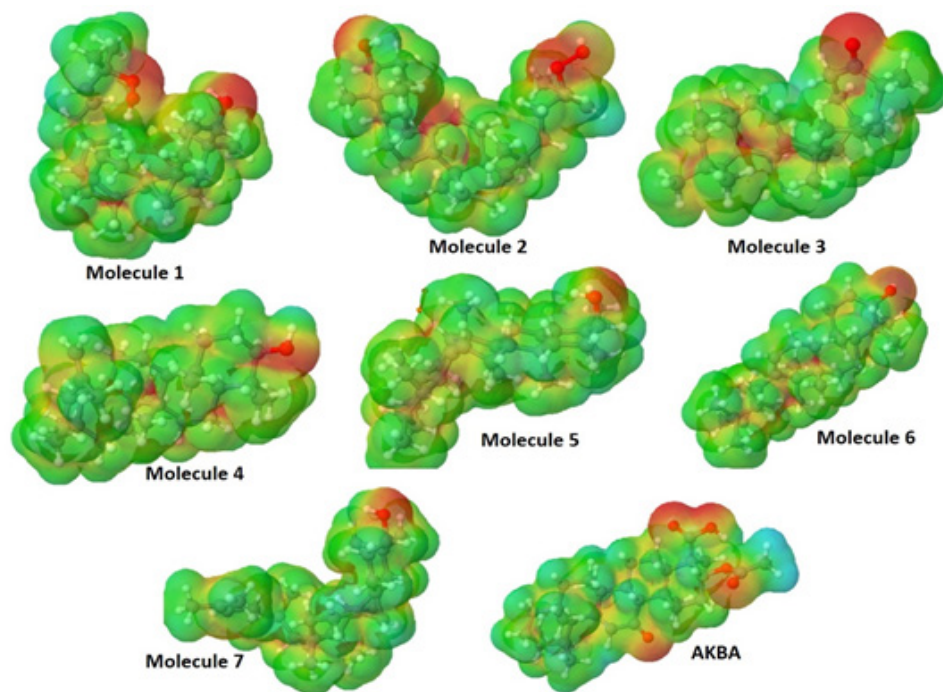
Figure 2. TESP mapping was obtained at the B3LYP/6-31(d) DFT level for the secondary metabolites investigated

Table IV.
Affinity Energy for AKBA and the triterpenes reported from *Euphorbia hirta* L.

Molecule	Affinity Energy (kcal/mol)
LOX-5 cristal ligand	-9,8
1	-7,2
2	-8,0
3	-8,6
4	-9,6
5	-8,4
6	-10,2
7	-7,8

68, VAL-110, HIS-130, ILE-126, GLN, 129 and LYS-133. The best mode of interaction for redocking showed an affinity energy of -9.8 kcal/mol calculated with AutoDock-Vina. For the series molecules in Figure 1, structure 6 showed a better stabilization affinity energy (-10.6 kcal/mol) (Figure 3c), highlighting interactions with the residues VAL-129, ARG-68, LEU-66, GLU-108, VAL-110, VAL-107, ILE-126, LYS-133, THR-137 and GLN-129. Structures 1 and 7 showed the lowest affinity energy, while the rest of the structures showed values comparable to those of the reference ligand (Table IV).

3.5 FMO CALCULATIONS

Figure 4 shows the Fragment molecular orbital method (FMO) analysis results of the triterpenes studied and their comparison with the crystallographic ligand reported for LOX-5. Each FMO analysis considered the residues of the best interaction mode according to molecular docking results. Additionally, Figure 5 shows the par interaction energies decomposition (PIEDA) in their electrostatic components, exchange, charge transfer, and dispersion. According

to the results, and in agreement with those reported by Gilbert et al. (2020), the AKBA ligand is mostly stabilized by interactions with residues LEU-66 (-8.453 kcal/mol), VAL-110 (-6.836 kcal/mol), and the HIS-130/GLN-129 (-16.871 kcal/mol). As seen in Figure 5, stabilization is mainly dominated by hydrophobic interactions (green bar). For amino acid residues such as VAL-110, electrostatic (blue bar) and charge transfer interactions (yellow bar) account for the hydrogen (N-O) bound between the residue and AKBA. In the case of the proposed molecules, some of the aforementioned interactions are preserved, and new ones appear as a result of the structural changes of each molecule.

For molecule 1, the best interaction is observed with the GLU-108/VAL-107 pair (-23.038 kcal/mol), which is dominated by dispersion interactions, while the energy
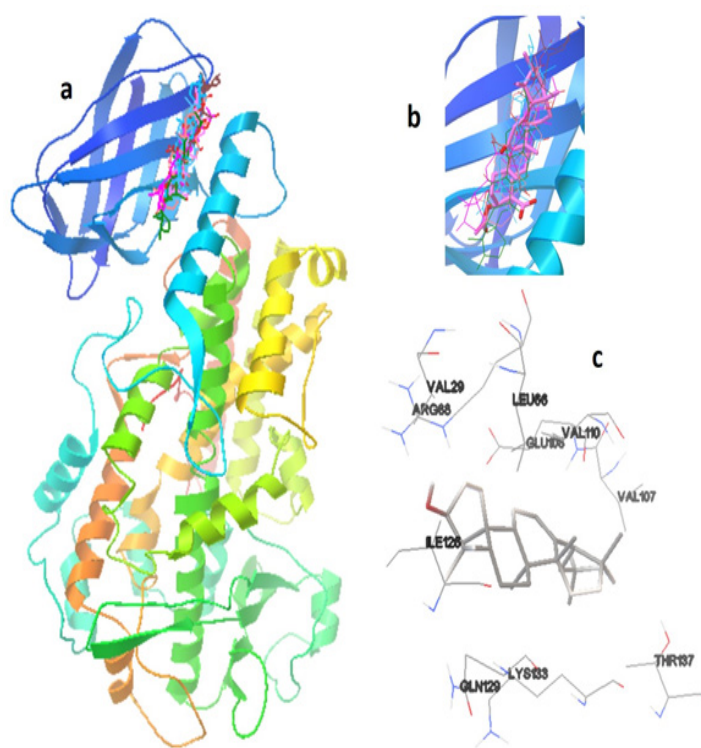
Figure 3. Redocking is used to reference the AKBA ligand (a, b) and the interaction mode for molecule 6 (c). All ligands were previously optimized at CAM-B3LYP/6-31(d) DFT level
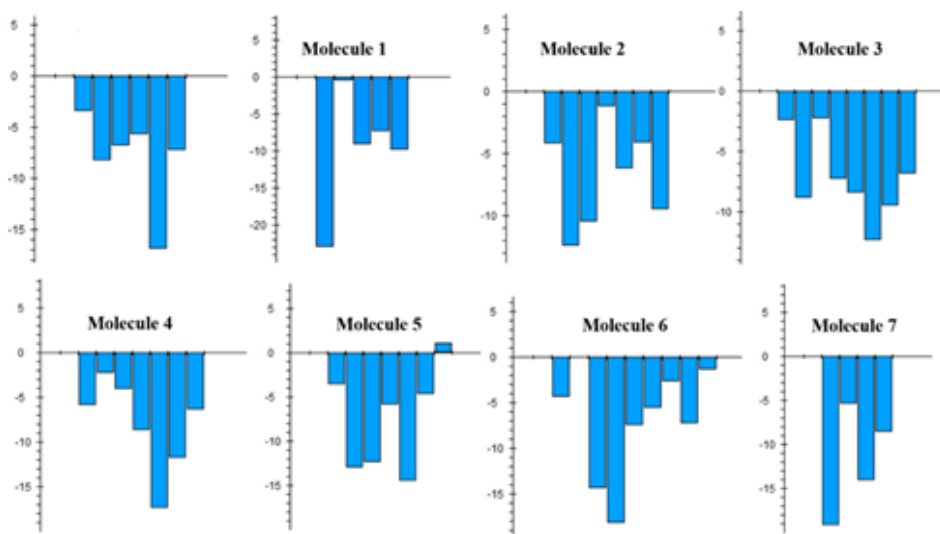
Figure 4. FMO analysis of the triterpenes studied and their comparison with the crystallographic ligand reported for LOX-5

interaction with VAL-110 significantly decreased. The decrease in the number of carboxylic groups in the ring system of structure 1 decreases the possibility of hydrogen bonding with VAL-110 and other residues. In fact, as shown in Figure S1 (supplementary material), the aliphatic chain and ring system are more exposed toward the GLU-108/VAL-107 residues, which justifies the stabilization by dispersion. In contrast, the -H atom in the terminal -OH group in the ring system is 3.38 Å from the N atom of VAL-110. For structure 1, interactions with THR-137 are also important (-7.38 kcal/mol), in agreement with Gilbert et al. (2020), and are dominated by dispersion interactions. According to our results (Figure 5 and Figure S1 in supplementary material), the contribution by charge transfer for the protein-molecule one complex, is justified by the coupling of the frontier orbitals (HOMO-molecule 1)/(LUMO-protein) between the aliphatic chain together with the terminal oxygen on the ligand (HOMO) and the amino acid fragment of GLU-134 (LUMO).

Molecule 2 shows significant agreement with the interacting fragments of LOX-5 with AKBA. In this case, ARG-68 (-12,433 kcal/mol) and ARG-101 (-10,523 kcal/mol) have the major stabilization energy. PIEDA results for ARG-101 show the highest stabilization by electrostatic and charge transfer contributions. Unlike molecule 1, and in accordance with AKBA, for molecule 2, VAL-110 shows the best contribution for the electrostatic terms (-13,698 kcal/mol), charge transfer (-34,492 kcal/mol), and dispersion (-18,455 kcal/mol). Figure S2 shows a hydrogen bridge between (VAL-110) -NH: OOHR-ligand (1.82 Å). On the other hand, the charge transfer contribution due to coupling of the orbital boundaries (HOMO-ligand)/(LUMO-LOX5) occurs between the aliphatic chain together with the terminal oxygens of the ligand (HOMO) and the amino acid fragment of LYS-133 (Figure S2).

Molecule 3 removes the aliphatic chain and terminal oxygen atoms from the -RHOO group, and the ring system is like AKBA.
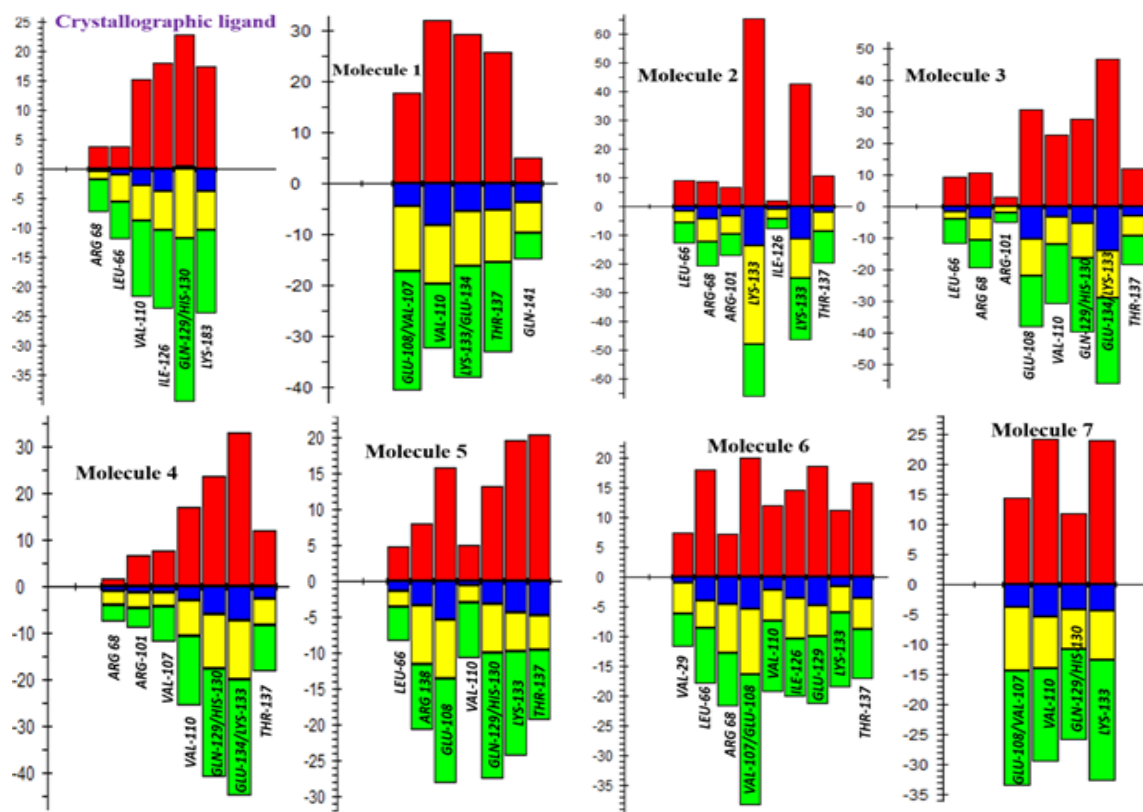
Figure 5. Interaction energies decomposition (PIEDA) in their electrostatic (blue bar), exchange (red bar), charge transfer (yellow bar), and dispersion (green bar) components
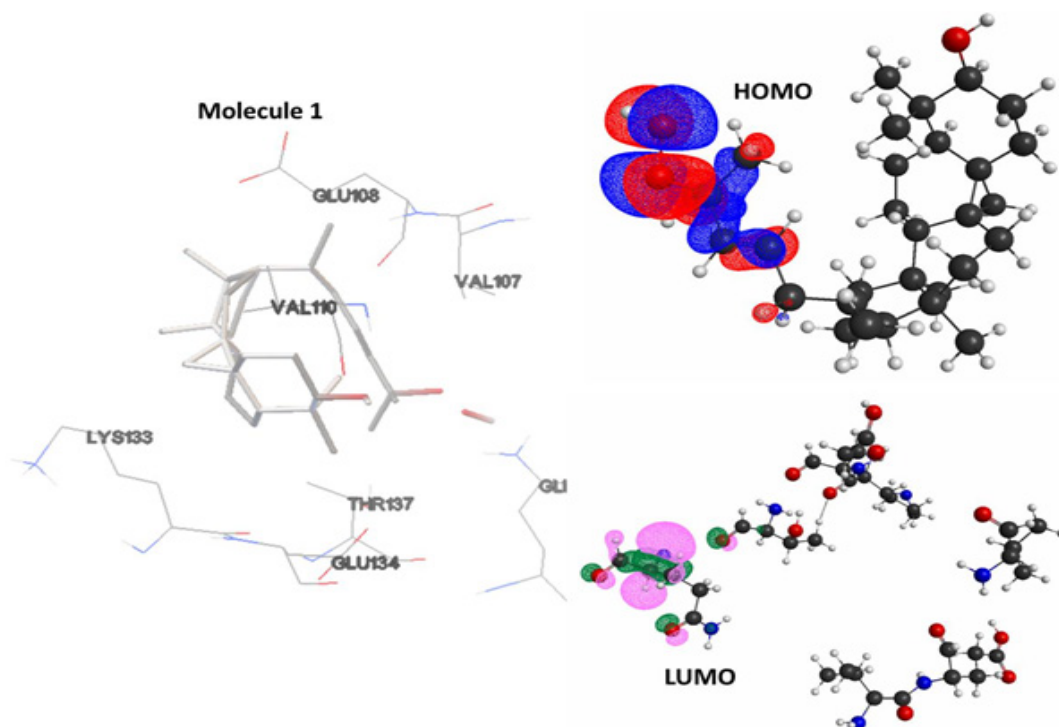
Figure S1. (Left side) Interaction mode between molecule 1 and LOX-5 active site (Top right side). HOMO in molecule 1 (Bottom right side). LUMO in the LOX-5 active site
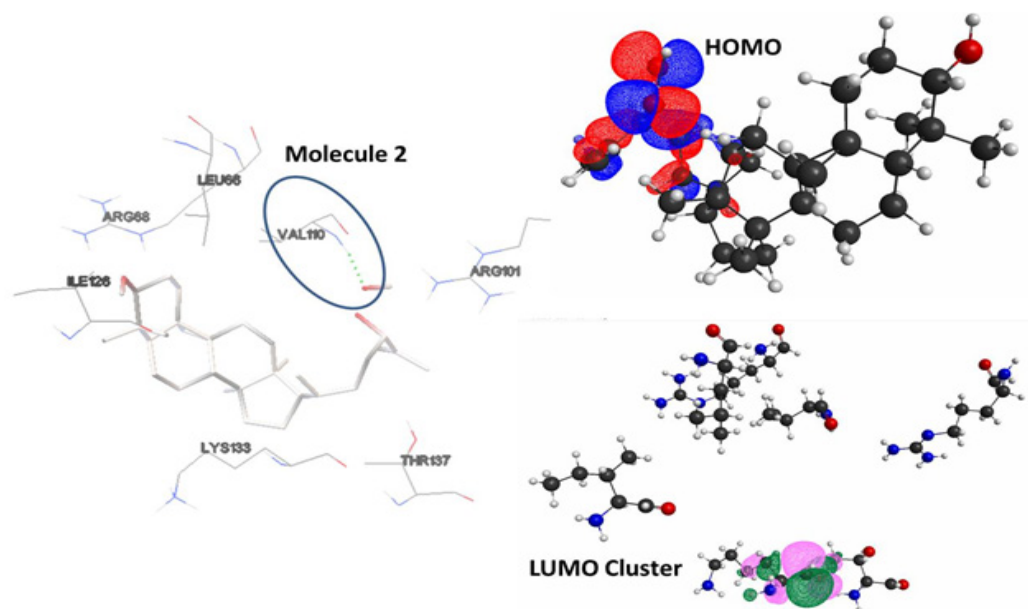
Figure S2. (Left side) Interaction mode between molecule 2 and LOX-5 active site (Top right side). HOMO in molecule 2 (Bottom right side). LUMO in the LOX-5 active site

This modification significantly increases the energy of interaction with VAL-110 (-8.413 kal/mol). GLU 188 (-7.295 kcal/mol) and ARG-68 (-8.888 kcal/mol) also contribute to the interaction energy. LYS-133 and GLU-134 were the fragments with the most stabilization due to charge transfer and dispersion effects. However, in this case, the LUMO orbital for the ligand-protein complex is located on HIS-130, while the HOMO orbital is extended in the ring system for the molecule 3 (Figure S3). The EI tendencies for molecule 4 are maintained for molecules 4 and 5. For molecule 5, the contribution by the exchange to the interaction energy in THR-137 exceeds the other contributions. It leads to a low energetic destabilization in relation to the remaining fragments (1.149 kcal/mol).

Molecular docking results show that structure 6 showed the best interaction energy (Table IV). Structure 6 shows the highest number of interacting fragments; some of these fragments coincide with those shown by AKBA. Additional fragments, such as VAL-29, VAL-107, and GLU-108, improve the interaction. For all the fragments, the electrostatic contribution to the interaction energy is significant in relation to the other structures. This trend is also present for charge transfer and dispersion. Hydrogen bonds are formed with VAL-29, ILE-126, LYS-133. The LUMO orbital is located on GLU-108, while the HOMO orbital is located along the ring system in molecule 6 (Figure S4). Finally, molecule 7 shows an aliphatic chain that decreases the number of interacting fragments. Its tendencies are similar to those observed in structure 1.

Conclusion

It was analyzed the bioavailability, bioactivity score, molecular similarity and molecular docking for seven secondary metabolites from *Euphorbia hirta* L., using as reference the structure of allosteric LOX-5 inhibitor 3-acetyl-11-keto-beta-boswellic
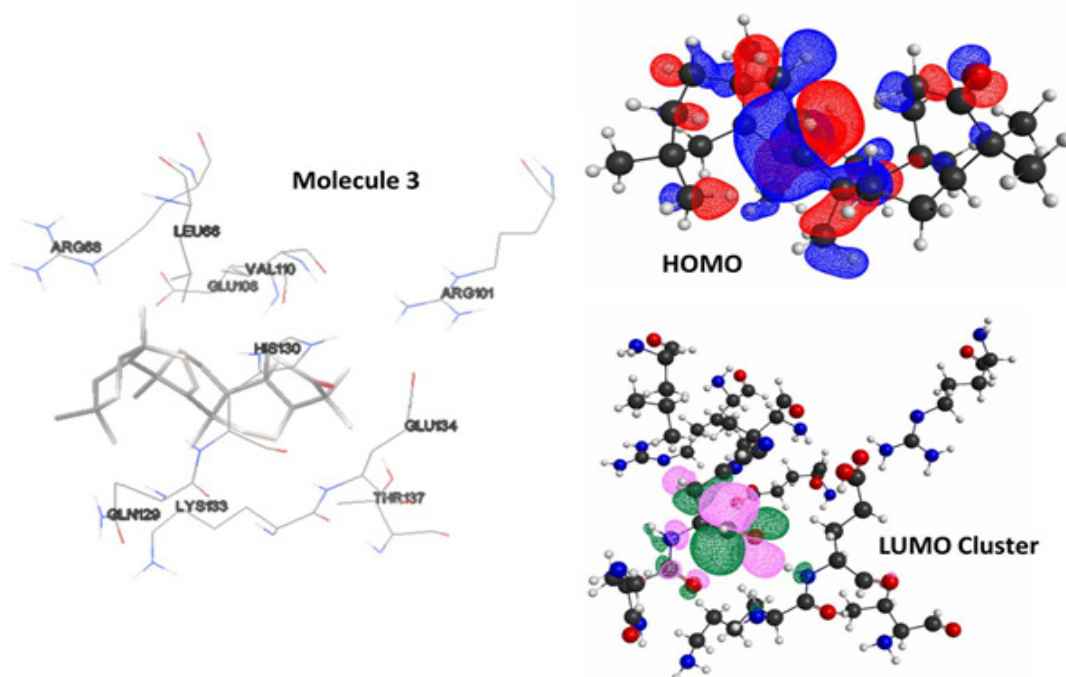
Figure S3. (Left side) Interaction mode between molecule 3 and LOX-5 active site (Top right side). HOMO in molecule 3 (Bottom right side). LUMO in the LOX-5 active site
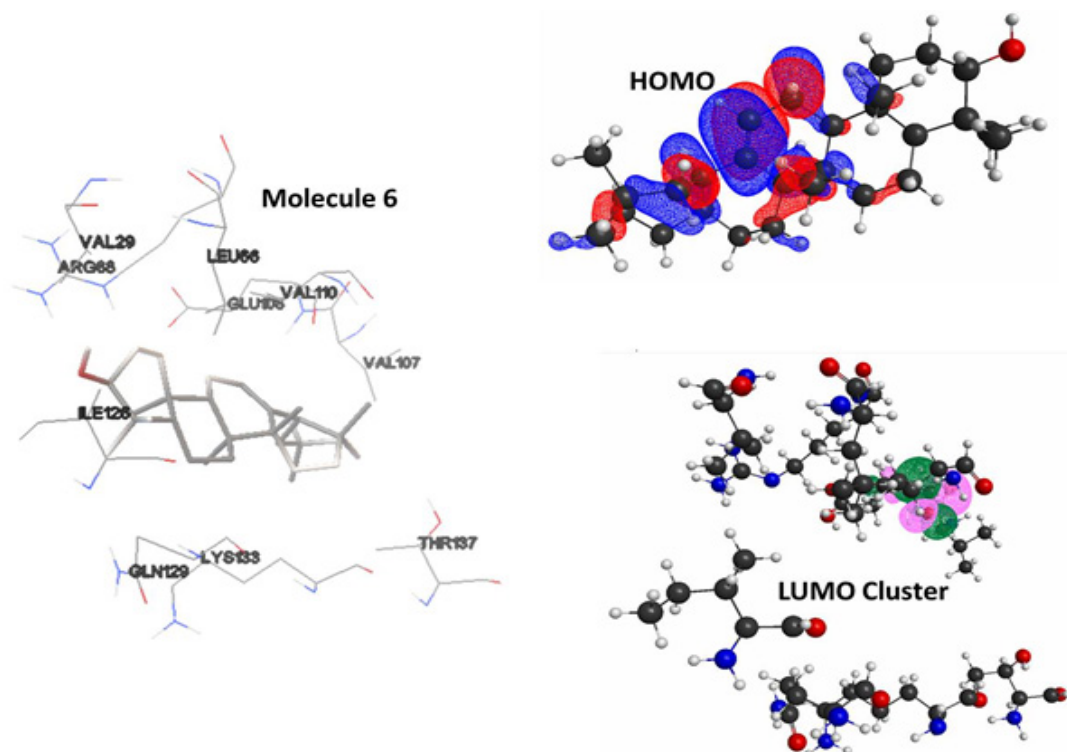
Figure S4. (Left side) Interaction mode between molecule 6 and LOX-5 active site (Top right side). HOMO in molecule 6 (Bottom right side). LUMO in the LOX-5 active site

acid (AKBA). The fragment molecular orbital method (FMO) and pair interaction energy decomposition analysis (PIEDA) were used to evaluate the interaction energy between secondary metabolites and the 5-LOX active site. Log P values of all the secondary metabolites studied were found to be higher than 5, contrary to what was expected with Lipinski's rules of five. However, the triterpenes metabolites studied can act primarily as nuclear receptor ligands and other enzyme inhibitors. Additionally, these molecules also can act moderately as GPCR ligands. The molecules studied have a good shape and ESP similarity with the reference ligand with values of 0.667 to 0.730. Both, AKBA and metabolites ligands were wedged between the two domains of LOX-5, and the main residues contact were LEU-66, ARG-68, VAL-110, HIS-130, ILE-126, GLN, 129 and LYS-133. The PIEDA analysis showed that stabilization in the 5-LOX active site is mainly dominated by hydrophobic interactions, with values up to -35 Kcal/mol. Due to the low presence of terminal -OH groups, electrostatic origin and charge transfer interaction energies are also important, but have values less than 20 Kcal/mol. Our results contribute to the molecular picture of the interaction mechanisms of secondary metabolites in *Euphorbia hirta* L. and reinforce the various experimental results on its possible use in inflammatory processes.

References

Anzline S, Israel S, Devi N, Sheeba RAJR, Rajkumar PR. 2017. High-resolution synchrotron powder diffraction study on charge density distribution of ampicillin trihydrate. Chin J Chem Phys 30: 50-62.

Anzline C, Israel S, Sujatha K, Sheeba RAJR. 2020. Hirshfeld surface, charge density and site selectivity studies of 1-(2-Methyl-5-nitro-1H-imidazol-1-yl)-acetone. Computational and Theoretical Chemistry 1191: 113044.

Bender A, Glen AC. 2004. Molecular similarity: a key technique in molecular informatics. Org Biomol Chem 2: 3204-3218.

Bennion BJ, Be NA, McNerney MW, Lao V, Carlson EM, Valdez CA, Malfatti MA, Enright HA, Nguyen TH, Lightstone FC, Carpenter TS. 2017. Predicting a drug's membrane permeability: a computational model validated with *in vitro* permeability assay data. J Phys Chem B 121: S228-S237.

Das K, Basheeruddin Asdaq SM, Saifulla Khan M, Amrutha S, Alamri A, Alhomrani M, Alsanie WF, Bhaskar A, Chandana Shree G, Harshitha P. 2022. Phytochemical investigation and evaluation of *in vitro* anti-inflammatory activity of *Euphorbia hirta* ethanol leaf and root extracts: A comparative study. Journal of King Saud University - Science 34: 102261.

Eckert H, Bajorath J. 2007. Molecular similarity analysis in virtual screening: foundations, limitations and novel approaches. Drug Discov Today 12: 225-233.

Fedorov DG, Kitaura K. 2006. Pair Interaction Energy Decomposition Analysis. Journal of Computational Chemistry 28: 222-237.

Fedorov DG, Kitaura K. 2012. Energy Decomposition Analysis in Solution Based on the Fragment Molecular Orbital Method. The Journal of Physical Chemistry A 116: 704-719.

Gadnayak A, Dehury B, Nayak A, Jena S, Sahoo A, Panda PC, Ray A, Nayak S. 2022. Mechanistic insights into 5-lipoxygenase inhibition by active principles derived from essential oils of Curcuma species: Molecular docking, ADMET analysis and molecular dynamic simulation study. PLoS One 17: e0271956.

Gasteiger J, Marsili M. 1980. Iterative partial equalization of orbital electronegativity - a rapid access to atomic charges. Tetrahedron 36(22): 3219–3228.

Ghansenyuy SY, Eyong KO, Yemback P, Mehreen L, Nziko, Vincent de Paul N, Ali Muhammad S. Folefoc GN. 2023. Lipoxygenase inhibition and molecular docking studies of secondary metabolites from the leaves of *Alstonia scholaris*. European Journal of Medicinal Chemistry Reports 9: 100108.

Gilbert NG, Gerstmeier J, Schexnaydre EE, Börner F, Garscha U, Neau DB, Werz O, Newcomer ME. 2020. Structural and mechanistic insights into 5-lipoxygenase inhibition by natural products. Nat Chem Biol 16: 783–790.

Grienke U, Mihály-Bison J, Schuster D, Afonyushkin T, Binder M, Guan S-H, Cheng C-R, Wolber G, Stuppner H, Guo D-A, Bochkov VN, Rollinger JM. 2011. Pharmacophore-based discovery of FXR-agonists. Part II: Identification of bioactive triterpenes from Ganoderma lucidum. Bioorganic & Medicinal Chemistry 19(22): 6779-6791.

Gonzalez R, Mroginski MA. 2019. Fully quantum chemical treatment of chromophore-protein interactions in phytochromes. J Phys Chem B 123(46): 9819-9830.

Hitchcock SA, Pennington LD. 2006. Structure−brain exposure relationships. J Med Chem. 49(26): 7559-7583.

Lipinski CA, Lombardo F, Dominy BW, Feeney PJ. 1997. Experimental and computational approaches to estimate solubility and permeability in drug discovery and development settings. Adv Drug Deliv Rev 23(1-3): 3-25.

Liu R, Zhang Y, Li S, Liu C, Zhuang S, Zhou X, Li Y, Zhang Y, Liang JY. 2023. Extraction and preparation of 5-lipoxygenase and acetylcholinesterase inhibitors from Astragalus membranaceus stems and leaves. Journal of Separation Science 46: 2200812.

Lončarić M, Strelec I, Moslavac T, Šubarić D, Pavić V, Molnar M. 2021. Lipoxygenase Inhibition by Plant Extracts. Biomolecules 11:152.

Nielsen DS, Shepherd NE, Weijun X, Lucke AJ, Stoermer MJ, Fairlie DP. 2017. Orally Absorbed Cyclic Peptides. Chemical Reviews 117(12): 8094-8128.

Pajouhesh H, Lenz GR. 2005. Medicinal chemical properties of successful central nervous system drugs. NeuroRx 2: 541-553.

Schmidt MW, Baldridge KK, Boatz JA, Elbert ST, Gordon MS, Jensen JA, Koseki S, Matsunaga N, Nguyen KA, Su S, Windus TL, Dupuis M, Montgomery Jr JA. 1993. General atomic and molecular electronic structure system. J Comput Chem 14(11): 1347-1363.

Molinspiration. 1986. Cheminformatics on the Web. Retrieved from http://www.molinspiration.com/

Muegge I. 2003. Selection criteria for drug-like compounds. Med Res Rev 23: 302-321.

Ochieng PJ, Sumaryada T, Okun D. 2017. Molecular docking and pharmacokinetic prediction of herbal derivatives as maltase-glucoamylase inhibitor. Asian J Pharm Clin Res 10(9):19337.

Pedretti A, Villa L, Vistoli G. 2004. VEGAZZ: an open platform to develop chemo-bio-informatics applications, using plug-in architecture and script programming. J Comput Aided Mol Des 18(3): 167–173.

Perri MJ, Weber SH. 2014. Web-Based job submission interface for the GAMESS computational chemistry program. J Chemical Education 91: 2206-2208.

Quynh Vo NN, Nomura Y, Muranaka T, Fukushima EO. 2019. Structure-activity relationships of pentacyclic triterpenoids as inhibitors of cyclooxygenase and lipoxygenase enzymes. J Natural Products 82(12): 3311-3320.

Rådmark A, Samuelsson B. 2009. 5-Lipoxygenase: mechanisms of regulation. J Lipid Research 50: 40-45.

Ragasa CY, Cornelio KB. 2013. Triterpenes from *Euphorbia hirta* and their cytotoxicity. Chinese Journal of Natural Medicines 11: 0528−0533.

Shi QW, Su XH, Kiyota H. 2008. Chemical and pharmacological research of the plants in Genus Euphorbia. Chemical Reviews 108(10): 4295-4327.

Shin W-H, Zhu X, Bures MG, Kihara D. 2015. Three-Dimensional Compound Comparison Methods and Their Application in Drug Discovery. Molecules 20(7): 12841-12862.

Schieferdecker S, König S, Koeberle A, Dahse HM, Werz O, Nett M. 2015. Myxochelins target human 5-lipoxygenase. J Nat Prod 78(2): 335–338.

Shi Q-W, Xiao-Hui Su, Hiromasa Kiyota. 2008. chemical and pharmacological research of the plants in Genus Euphorbia. Chemical Review 108: 4295-4327.

Siraj MA, Rahman MS, Tan GT, Seidel V. 2021. Molecular docking and molecular dynamics simulation studies of Triterpenes from *Vernonia patula* with the Cannabinoid Type 1 Receptor. International J Molecular Sciences 22(7): 3595.

Suenaga M. 2005. Facio: New Computational Chemistry Environment for PC GAMESS. J Computer Chemistry, Japan 4: 25-32.

Trott O, Olson AJ. 2010. AutoDock Vina: improving the speed and accuracy of docking with a new scoring function, efficient optimization and multithreading. J Computational Chemistry 31(2): 455-461.

Vainio MJ, Puranen JS, Johnson MS. 2009. ShaEP: molecular overlay based on shape and electrostatic potential. J Chem Inf Model 49(2): 492-502.

Veber D, Johnson SR, Cheng H-Y, Smith BR, Ward KW Koppl KD. 2002. Molecular properties that influence the oral bioavailability of drug candidates. J Med Chem 45(12): 2615-2623.

Verma RK. 2017. A review - taxonomical study and medicinal uses of *Euphorbia hirta* (Linn.)

in churu Rajasthan. World J Pharm Res 6(10): 1320–2134.

Wang Q, Qiao X, Qian Y, Li Z, Zhou D, Guo D, Ye M. 2015. Intestinal absorption of ergostane and lanostane triterpenoids from Antrodia cinnamomea using Caco-2 cell monolayer model. Nat Prod Bioprospect 5: 237–246.

Yamaguchi H, Yu T, Noshita T, Kidachi Y, Kamiie K, Yoshida K. 2011. Ligand-receptor Interaction between triterpenoids and the hydroxysteroid dehydrogenase type 2 enzyme predicts their toxic effects against tumorigenic r/m HM-SFME-1 cells J Biol Chem 286: 36888–36897.

Zhao L, Zhou S, Gustafsson JÅ. 2019. Nuclear receptors: recent drug discovery for cancer therapies. Endocrine Reviews 40: 1207–1249.